

**EXPERIMENTAL INVESTIGATIONS INTO CHARACTERIZATION
AND MACHINING PERFORMANCE OF CUTTING TOOL INSERTS
FABRICATED BY DIRECTED ENERGY DEPOSITION**

NEETESH KUMAR SAH



**DEPARTMENT OF MECHANICAL ENGINEERING
INDIAN INSTITUTE OF TECHNOLOGY DELHI**

MARCH 2026

©Indian Institute of Technology Delhi (IITD), New Delhi, 2026

**EXPERIMENTAL INVESTIGATIONS INTO CHARACTERIZATION
AND MACHINING PERFORMANCE OF CUTTING TOOL INSERTS
FABRICATED BY DIRECTED ENERGY DEPOSITION**

by

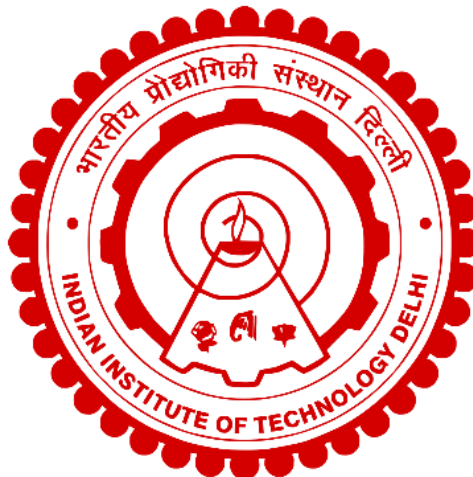
NEETESH KUMAR SAH

DEPARTMENT OF MECHANICAL ENGINEERING

Submitted

In fulfilment of the requirements of the degree of Doctor of Philosophy

to the



INDIAN INSTITUTE OF TECHNOLOGY DELHI

MARCH 2026

DEDICATED TO

MY FAMILY AND LOVED ONES

Certificate

This is to certify that the thesis entitled '**Experimental investigations into characterization and machining performance of cutting tool inserts fabricated by directed energy deposition**' submitted by **Mr. Neetesh Kumar Sah** to the Indian Institute of Technology Delhi, for the award of the degree of *Doctor of Philosophy*, is a record of the original bonafide research work carried out by him under my guidance and supervision. The results contained in it have not been submitted in part or full to any other institute or university for the award of any degree/diploma.



(Dr. Pulak Mohan Pandey)

IHFC Chair, Professor (HAG)

Department of Mechanical Engineering

Indian Institute of Technology Delhi



(Dr. Sudarsan Ghosh)

Professor (HAG)

Department of Mechanical Engineering

Indian Institute of Technology Delhi



(Dr. Gurminder Singh)

Assistant Professor

Department of Mechanical Engineering

Indian Institute of Technology Bombay

Date: 24-03-2026

Acknowledgements

This thesis symbolizes an important milestone in the journey of my life. I express my deep sense of gratitude and sincere thanks to my thesis supervisors ***Prof. Pulak M. Pandey***, ***Prof. Sudarsan Ghosh***, and ***Prof. Gurminder Singh***. Their excellent guidance, constant encouragement, and optimistic outlook have been a source of motivation for me throughout this work. Their insightful advice and constructive feedback have been instrumental in shaping this research. Their knowledge of the subject and wealth of experience steered me to complete the work. My interaction with them has been a great learning experience. I am truly grateful for the countless hours they have spent discussing ideas, reviewing my work, and helping me navigate the challenges of this journey. Besides being a source of immense knowledge and experience, ***Prof. Pulak M. Pandey***, ***Prof. Sudarsan Ghosh***, and ***Prof. Gurminder Singh*** are very kind and caring with great compassion and love for the students. Their mentorship has not only enhanced my research skills but also inspired me to strive for excellence in all aspects of my academic and professional life. I will forever cherish my close association with them.

I express my deep sense of gratitude to ***Prof. Sunil Jha***, ***Prof. R. K. Pandey***, and ***Prof. S. Fatima*** for being part of my student research committee and thankful for their constructive criticism and valuable guidance during the course of presentations. I am thankful to the lab staff members ***Mr. Paras Gupta***, ***Mr. Abhishek Rana***, ***Mr. Subhash Chand***, and ***Mr. Roshan Lal*** for providing me with essential aids to complete experimentation work for the thesis. I am grateful to the operational in-charge, ***Dr. Ravinder Kumar***, ***Mr. Kuldeep Sharma***, and ***Mr. Dinesh Kumar*** of the central research facility (CRF) for providing me with essential aids to complete experimentation work for the thesis. I would also like to thank ***Prof. Ramesh Singh, IIT Bombay***, for allowing access to the DED facility used for sample preparation.

I am also thankful to the office staff members *Mr. Kishan Kumar, Ms. Nida Ansari, Mr. Sonu Gaur, and Mr. Naveen Kumar* for their support in the day-to-day activities. I extend my sincere thanks to my friends and research scholars at IIT Delhi, *Dr. Rudranarayan Kandi, Dr. Arun Kumar, Dr. Shitanshu Arya, Dr. Gaurav Tripathi, Dr. Garima Dixit, Dr. Priyabrata Das, Dr. Patel Brijeshkumar Hasmukhbhai, Dr. Shubham Shankar Mohol, Dr. Snehal Arun Shende, Dr. Shravan Kumar Yadav, Dr. Gaurav Sharma, Ms. Arti Sahu, Mr. Rakesh Kandulna, Mr. Amal Gupta, Mr. Amey Parnaik, Mr. Nitin Srivastava, Mr. Sudarshan P. Gajre* and co-research scholars/friends who were always there to lend a helping hand when it mattered the most and for the camaraderie that took away all the pressures and made research work more enjoyable. I am deeply grateful to my M.Tech supervisor *Prof. Varun Sharma, IIT Roorkee*, whose mentorship and support played a significant role in shaping my research career.

I am indebted to my parents, *Shri. Haricharan Sah and Smt. Ramawati Devi* for their blessings, motivation, and constant support throughout this period. I appreciate the love and support of all my family members for their kind cooperation, great inspiration, providing me with moral support, and taking care of all the social responsibilities. I am thankful to everyone who helped me directly or indirectly to complete this work. I am also grateful to *God, the Almighty*, for having blessed me to rise and take up this challenge.

(Neetesh Kumar Sah)

Abstract

Machining is one of the most widely adopted manufacturing processes for producing high-performance components with precise geometry, high dimensional accuracy, and excellent surface quality. The machining performance under dry conditions strongly depends on the cutting tool materials. M2 high-speed steel (M2 HSS) is a cost-effective and commonly used tool material owing to its high hardness, good wear resistance, remarkable hot hardness, and adequate toughness. Despite these advantages, its applicability is limited in high-speed machining and specifically in machining difficult-to-cut materials. Therefore, the performance of M2 HSS needs to be improved to meet the increasing demands of modern machining applications. The incorporation of ceramic reinforcements is recognized as an effective approach for significantly improving the hardness and wear resistance of M2 HSS. In the present study, boron carbide (B_4C) was selected as the reinforcement material owing to its extremely high hardness, excellent chemical stability, and ability to maintain high hardness at elevated temperatures, which enhances the hardness and wear resistance of the metal matrix. Therefore, M2 HSS- B_4C composite was developed for advanced cutting tool applications.

The fabrication of composite cutting tools using traditional manufacturing routes such as powder metallurgy poses several challenges, including numerous processing steps, extended lead times, material wastage, incomplete densification due to the use of binders, and difficulties in fabricating intricate geometries. To overcome these limitations, directed energy deposition (DED) emerges as a technologically advanced metal-based additive manufacturing (AM) process capable of fabricating near-net-shape and fully dense metallic objects with high material efficiency and design flexibility with significantly reduced processing steps. Therefore, this study explores the feasibility and potential of the DED process for fabricating M2 HSS- B_4C composite cutting tool inserts.

The selection of suitable DED process parameters is a crucial step for producing defect-free and high-quality components. Therefore, the DED process was first used to manufacture M2 HSS specimens with a focus on understanding the influence of key process parameters on the geometrical features of single-track depositions. Based on the preferred range of dilution and aspect ratio for high-quality depositions, the most suitable process parameters were determined as a laser power of 1600 W, a scan speed of 500 mm/min, and a powder feed rate of 12 g/min. Furthermore, a multilayer M2 HSS component fabricated under these selected parameters was characterized for microstructure and phase analysis, which indicated the presence of martensite, retained austenite, and eutectic carbide phases. The DED-fabricated M2 HSS exhibited a microhardness of approximately 734 ± 12 HV.

Subsequently, the DED parameters selected based on the single-bead deposition study were used to fabricate M2 HSS-B₄C composite samples containing 0-20 vol.% B₄C. The influence of B₄C addition on microstructure, phase formation, microhardness, and wear behavior were systematically investigated and compared with unreinforced M2 HSS. The microstructure and phase analysis revealed that the incorporation of B₄C reinforcement into the M2 HSS matrix facilitated the in-situ formation of hard ceramic phases such as iron borides (FeB and Fe₂B) and iron carbide (Fe₃C) in addition to the martensite, retained austenite, and M₂C-type carbide. The microhardness result demonstrated a substantial increase from ~734 HV for unreinforced M2 HSS to ~1034 HV for the composite containing 20 vol.% B₄C, representing an improvement of nearly 41%. This enhancement is primarily attributed to grain refinement, solid-solution strengthening, and the presence of hard ceramic phases induced by the B₄C reinforcement. The wear characteristics were evaluated in terms of coefficient of friction, mass loss, and wear rate. Further, the wear mechanism and surface topography were analysed using scanning electron microscopy (SEM) and a 3D profilometer. The wear results revealed that increasing B₄C contents effectively decreased the mass loss and wear rate with a

maximum reduction of approximately 73% and 68%, respectively, for the composite containing 20 vol.% B₄C relative to the unreinforced M2 HSS. The dominant wear mechanism in the composite sample was transitioned from adhesive to abrasive type. The findings indicated an improvement in wear resistance of the composite samples with increasing B₄C content.

Thereafter, cutting tool inserts of M2 HSS-B₄C composite materials were developed using the DED process and the machining performance was investigated through turning AISI 1045 steel. The study focused on investigating the influence of machining parameters and determining optimal conditions to achieve superior machining performance. Statistical predictive models were developed using response surface methodology (RSM) to correlate machining response variables such as cutting force, surface roughness, and tool wear with machining parameters and B₄C content. Subsequently, a multi-objective optimization was performed using a genetic algorithm to optimize the machining parameters and B₄C content, aiming to minimize the response variables. The optimal machining conditions were identified as a cutting speed of 53.12 m/min, a feed rate of 0.07 mm/rev, and a depth of cut of 0.13 mm, along with an optimized B₄C content of 11.13 vol.%. Finally, the machining performance under the optimized conditions was compared with that of conventional M2 HSS cutting tools. The findings indicated that the DED-fabricated M2 HSS-11.13 vol.% B₄C composite cutting tool achieved significant performance enhancements, exhibiting reductions of 28.8%, 30%, and 24.4% in resultant cutting force, surface roughness, and tool flank wear, respectively, compared to the conventional M2 HSS tool. Additionally, corresponding reductions of 20.7%, 19.3%, and 16.8% were observed when compared with DED-fabricated unreinforced M2 HSS cutting tools. These results clearly indicate that the incorporation of B₄C reinforcement into M2 HSS significantly improves the machining performance of the cutting inserts.

Finally, the present work was extended to deposit TiN and AlTiN surface coatings on the optimized DED-fabricated M2 HSS-11.13 vol.% B₄C cutting inserts using physical vapor

deposition (PVD) to further enhance the machining performance. Both coatings exhibited uniform, continuous, and crack-free deposition, along with some microvoids and droplets observed on the surfaces. The XRD patterns revealed the presence of TiN and AlTiN phases with face-centered cubic (FCC) crystal structures. Compared to the uncoated tool, the TiN- and AlTiN-coated tools showed improvements in microhardness of approximately 21% and 52%, respectively. The performance of the coated tools was further evaluated through turning AISI 1045 steel under the optimized machining parameters. The results demonstrated that the use of TiN-coated tools reduced the cutting force, surface roughness, and tool flank wear by approximately 21%, 18%, and 24%, respectively, compared to the uncoated tools. In contrast, the AlTiN-coated tools exhibited a corresponding reduction of about 38%, 31%, and 41%. Furthermore, the application of TiN and AlTiN coatings achieved improvements in tool life of approximately 34% and 59%, respectively, compared to the uncoated tool. Overall, the AlTiN-coated cutting inserts exhibited superior machining performance compared to both TiN-coated and uncoated inserts.

सार

मशीनिंग सटीक ज्यामिति, उच्च आयामी सटीकता और उत्कृष्ट सतह गुणवत्ता वाले उच्च-प्रदर्शन वाले कंपोनेंट बनाने के लिए सबसे व्यापक रूप से अपनाई जाने वाली निर्माण प्रक्रियाओं में से एक है। सूखी स्थितियों में मशीनिंग का प्रदर्शन काफी हद तक कटिंग टूल सामग्री पर निर्भर करता है। M2 हाई-स्पीड स्टील (M2 HSS) अपनी उच्च कठोरता, अच्छे घिसाव प्रतिरोध, उल्लेखनीय गर्म कठोरता और पर्याप्त मजबूती के कारण एक लागत प्रभावी और आमतौर पर इस्तेमाल की जाने वाली टूल सामग्री है। इन फायदों के बावजूद, इसकी उपयोगिता हाई-स्पीड मशीनिंग में और विशेष रूप से मुश्किल से काटे जाने वाले पदार्थों की मशीनिंग में सीमित है। इसलिए, आधुनिक मशीनिंग अनुप्रयोगों की बढ़ती मांगों को पूरा करने के लिए M2 HSS के प्रदर्शन में सुधार करने की आवश्यकता है। सिरेमिक रीइन्फोर्समेंट को शामिल करना M2 HSS की कठोरता और घिसाव प्रतिरोध में काफी सुधार करने के लिए एक प्रभावी तरीका माना जाता है। वर्तमान अध्ययन में, बोरॉन कार्बाइड (B₄C) को रीइन्फोर्समेंट सामग्री के रूप में चुना गया था क्योंकि इसकी अत्यधिक उच्च कठोरता, उत्कृष्ट रासायनिक स्थिरता और उच्च तापमान पर उच्च कठोरता बनाए रखने की क्षमता है, जो धातु मैट्रिक्स की कठोरता और घिसाव प्रतिरोध को बढ़ाती है। इसलिए, उन्नत कटिंग टूल अनुप्रयोगों के लिए M2 HSS-B₄C कंपोजिट विकसित किया गया था।

पाउडर धातुकर्म जैसे पारंपरिक निर्माण मार्गों का उपयोग करके कंपोजिट कटिंग टूल का निर्माण कई चुनौतियाँ पेश करता है, जिसमें कई प्रसंस्करण चरण, विस्तारित लीड टाइम, सामग्री की बर्बादी, बाइंडर के उपयोग के कारण अधूरा घनत्व और जटिल ज्यामिति के निर्माण में कठिनाइयाँ शामिल हैं। इन सीमाओं को दूर करने के लिए, डायरेक्टेड एनर्जी डिपोजिशन (DED) एक तकनीकी रूप से उन्नत धातु-आधारित एडिटिव मैनुफैक्चरिंग (AM) प्रक्रिया के रूप में उभरता है जो उच्च सामग्री दक्षता और डिजाइन लचीलेपन के साथ लगभग नेट-शेप और पूरी तरह से घने धात्विक वस्तुओं का निर्माण करने में सक्षम है, जिसमें प्रसंस्करण चरणों में काफी कमी आती है। इसलिए, यह अध्ययन M2 HSS-

B₄C कंपोजिट कटिंग टूल इंसर्ट के निर्माण के लिए DED प्रक्रिया की व्यवहार्यता और क्षमता की पड़ताल करता है।

दोष-मुक्त और उच्च-गुणवत्ता वाले कंपोनेंट बनाने के लिए उपयुक्त DED प्रक्रिया मापदंडों का चयन एक महत्वपूर्ण कदम है। इसलिए, DED प्रक्रिया का उपयोग पहले M2 HSS नमूनों के निर्माण के लिए किया गया था, जिसमें सिंगल-ट्रैक डिपोजिशन की ज्यामितीय विशेषताओं पर प्रमुख प्रक्रिया मापदंडों के प्रभाव को समझने पर ध्यान केंद्रित किया गया था। उच्च-गुणवत्ता वाले डिपोजिशन के लिए डाइल्यूशन और पहलू अनुपात की पसंदीदा सीमा के आधार पर, सबसे उपयुक्त प्रक्रिया मापदंडों को 1600 W की लेजर शक्ति, 500 mm/min की स्कैन गति और 12 g/min की पाउडर फीड दर के रूप में निर्धारित किया गया था। इसके अलावा, इन चुने हुए पैरामीटर के तहत बनाए गए एक मल्टीलेयर M2 HSS कंपोनेंट का माइक्रोस्ट्रक्चर और फेज़ एनालिसिस किया गया, जिससे मार्टेंसाइट, रिटेन्ड ऑस्टेनाइट और यूटेक्टिक कार्बाइड फेज़ की मौजूदगी का पता चला। DED-निर्मित M2 HSS में लगभग 734 ± 12 HV की माइक्रोहार्डनेस पाई गई।

इसके बाद, सिंगल-बीड डिपोजिशन स्टडी के आधार पर चुने गए DED पैरामीटर का उपयोग करके 0-20 वॉल्यूम% B₄C वाले M2 HSS-B₄C कंपोजिट सैंपल बनाए गए। माइक्रोस्ट्रक्चर, फेज़ फॉर्मेशन, माइक्रोहार्डनेस और वियर बिहेवियर पर B₄C मिलाने के प्रभाव की व्यवस्थित रूप से जांच की गई और इसकी तुलना बिना रीइन्फोर्समेंट वाले M2 HSS से की गई। माइक्रोस्ट्रक्चर और फेज़ एनालिसिस से पता चला कि M2 HSS मैट्रिक्स में B₄C रीइन्फोर्समेंट को शामिल करने से मार्टेंसाइट, रिटेन्ड ऑस्टेनाइट और M₂C-प्रकार के कार्बाइड के अलावा आयरन बोराइड (FeB और Fe₂B) और आयरन कार्बाइड (Fe₃C) जैसे कठोर सिरैमिक फेज़ का इन-सीटू निर्माण आसान हो गया। माइक्रोहार्डनेस के परिणाम से पता चला कि बिना रीइन्फोर्समेंट वाले M2 HSS के लिए ~734 HV से बढ़कर 20 वॉल्यूम% B₄C वाले कंपोजिट के लिए ~1034 HV हो गया, जो लगभग 41% का सुधार

दर्शाता है। यह सुधार मुख्य रूप से ग्रेन रिफाइनमेंट, सॉलिड-सॉल्यूशन स्ट्रेंथनिंग और B₄C रीइन्फोर्समेंट द्वारा प्रेरित कठोर सिरेमिक फेज़ की उपस्थिति के कारण है। वियर विशेषताओं का मूल्यांकन घर्षण गुणांक, द्रव्यमान हानि और वियर दर के संदर्भ में किया गया। इसके अलावा, वियर मैकेनिज्म और सतह की स्थलाकृति का विश्लेषण स्कैनिंग इलेक्ट्रॉन माइक्रोस्कोपी (SEM) और 3D प्रोफाइलोमीटर का उपयोग करके किया गया। वियर के परिणामों से पता चला कि B₄C की मात्रा बढ़ाने से द्रव्यमान हानि और वियर दर में प्रभावी रूप से कमी आई, जिसमें बिना रीइन्फोर्समेंट वाले M2 HSS की तुलना में 20 वॉल्यूम% B₄C वाले कंपोजिट के लिए क्रमशः लगभग 73% और 68% की अधिकतम कमी देखी गई। कंपोजिट सैंपल में प्रमुख वियर मैकेनिज्म एडहेसिव से एब्रेसिव प्रकार में बदल गया। निष्कर्षों से पता चला कि B₄C की मात्रा बढ़ने के साथ कंपोजिट सैंपल के वियर रेजिस्टेंस में सुधार हुआ।

इसके बाद, DED प्रक्रिया का उपयोग करके M2 HSS-B₄C कंपोजिट सामग्री के कटिंग टूल इंsert विकसित किए गए और AISI 1045 स्टील की टर्निंग करके मशीनिंग प्रदर्शन की जांच की गई। अध्ययन में मशीनिंग पैरामीटर के प्रभाव की जांच करने और बेहतर मशीनिंग प्रदर्शन प्राप्त करने के लिए इष्टतम स्थितियों को निर्धारित करने पर ध्यान केंद्रित किया गया। रिस्पॉन्स सरफेस मेथोडोलॉजी (RSM) का इस्तेमाल करके स्टैटिस्टिकल प्रेडिक्टिव मॉडल विकसित किए गए ताकि कटिंग फोर्स, सरफेस रफनेस और टूल वियर जैसे मशीनिंग रिस्पॉन्स वेरिएबल को मशीनिंग पैरामीटर और B₄C कंटेंट से जोड़ा जा सके। इसके बाद, रिस्पॉन्स वेरिएबल्स को कम करने के मकसद से मशीनिंग पैरामीटर्स और B₄C कंटेंट को ऑप्टिमाइज़ करने के लिए जेनेटिक एल्गोरिदम का इस्तेमाल करके मल्टी-ऑब्जेक्टिव ऑप्टिमाइज़ेशन किया गया। ऑप्टिमल मशीनिंग कंडीशंस को 53.12 m/min की कटिंग स्पीड, 0.07 mm/rev की फीड रेट और 0.13 mm की कट की गहराई के साथ-साथ 11.13 vol.% के ऑप्टिमाइज़्ड B₄C कंटेंट के रूप में पहचाना गया। आखिर में, ऑप्टिमाइज़्ड कंडीशंस के तहत मशीनिंग परफॉर्मेंस की तुलना पारंपरिक M2 HSS कटिंग टूल्स से की गई। नतीजों से पता चला कि DED-फैब्रिकेटेड M2 HSS-11.13 vol.% B₄C कम्पोजिट कटिंग टूल ने पारंपरिक M2 HSS टूल की तुलना में रिजल्टेंट कटिंग फोर्स,

सरफेस रफनेस और टूल फ्लैक वियर में क्रमशः 28.8%, 30% और 24.4% की कमी दिखाते हुए परफॉर्मेंस में काफी सुधार हासिल किया। इसके अलावा, DED-फैब्रिकेटेड अनरिनफोर्स्ड M2 HSS कटिंग टूल्स की तुलना में 20.7%, 19.3% और 16.8% की संबंधित कमी देखी गई। ये नतीजे साफ तौर पर बताते हैं कि M2 HSS में B₄C रीइन्फोर्समेंट को शामिल करने से कटिंग इंसर्ट की मशीनिंग परफॉर्मेंस में काफी सुधार होता है।

आखिर में, इस काम को ऑप्टिमाइज़्ड DED-फैब्रिकेटेड M2 HSS-11.13 vol.% B₄C कटिंग इंसर्ट पर फिजिकल वेपर डिपोजिशन (PVD) का इस्तेमाल करके TiN और AlTiN सरफेस कोटिंग्स जमा करने के लिए बढ़ाया गया ताकि मशीनिंग परफॉर्मेंस को और बेहतर बनाया जा सके। दोनों कोटिंग्स ने सतहों पर कुछ माइक्रोवाइंड्स और ड्रॉपलेट्स के साथ एक समान, लगातार और क्रैक-फ्री डिपोजिशन दिखाया। XRD पैटर्न ने फेस-सेंटरड क्यूबिक (FCC) क्रिस्टल स्ट्रक्चर के साथ TiN और AlTiN चरणों की उपस्थिति का खुलासा किया। बिना कोटेड टूल की तुलना में, TiN- और AlTiN-कोटेड टूल्स ने माइक्रोहार्डनेस में क्रमशः लगभग 21% और 52% का सुधार दिखाया। कोटेड टूल्स के परफॉर्मेंस का मूल्यांकन ऑप्टिमाइज़्ड मशीनिंग पैरामीटर्स के तहत AISI 1045 स्टील को टर्निंग करके किया गया। नतीजों से पता चला कि बिना कोटिंग वाले टूल्स की तुलना में TiN-कोटेड टूल्स के इस्तेमाल से कटिंग फोर्स, सरफेस रफनेस और टूल फ्लैक वियर में क्रमशः लगभग 21%, 18% और 24% की कमी आई। इसके उलट, AlTiN-कोटेड टूल्स में इसी तरह लगभग 38%, 31% और 41% की कमी देखी गई। इसके अलावा, बिना कोटिंग वाले टूल की तुलना में TiN और AlTiN कोटिंग के इस्तेमाल से टूल लाइफ में क्रमशः लगभग 34% और 59% का सुधार हुआ। कुल मिलाकर, AlTiN-कोटेड कटिंग इंसर्ट ने TiN-कोटेड और बिना कोटिंग वाले दोनों इंसर्ट की तुलना में बेहतर मशीनिंग परफॉर्मेंस दिखाया।

Table of Contents

Certificate.....	i
Acknowledgements.....	ii
Abstract.....	iv
सार.....	viii
Table of Contents	xii
List of Figures.....	xvii
List of Tables.....	xxi
Abbreviations.....	xxii
Nomenclature.....	xxv
Chapter 1 Introduction.....	1
1.1 Introduction.....	2
1.1.1 Machining	2
1.1.2 Powder metallurgy	5
1.1.2.1 Hot pressing	5
1.1.2.2 Spark plasma sintering.....	7
1.1.2.3 Microwave sintering	8
1.1.3 Additive manufacturing	10
1.1.3.1 Selective laser melting	11
1.1.3.2 Directed energy deposition	13
1.1.4 Cutting tool coating.....	15
1.1.4.1 Chemical vapor deposition	16
1.1.4.2 Physical vapor deposition	17

1.2	Motivation for the current study	19
1.3	Thesis organization	22
Chapter 2	Literature review and research objectives.....	25
2.1	Literature review	26
2.1.1	Cutting tool inserts fabrication using powder metallurgy processes	26
2.1.2	Cutting tool inserts fabrication using additive manufacturing processes	31
2.1.2.1	Indirect metal AM process	31
2.1.2.2	Direct metal AM process	33
2.1.3	Coating of cutting tool inserts.....	35
2.1.4	Optimization of machining process parameters.....	37
2.2	Research gaps.....	39
2.3	Proposed research work and objectives	40
Chapter 3	Effects of DED process parameters on single bead geometry	41
3.1	Introduction.....	42
3.2	Materials and methods	44
3.2.1	Materials	44
3.2.2	Directed energy deposition process	45
3.2.3	Characterization of single bead deposition	46
3.2.4	Characterization of multilayer deposition.....	47
3.3	Results and discussion	48
3.3.1	Single bead deposition	48
3.3.2	Effect of process parameters on bead width, height, and penetration depth....	51
3.3.3	Effect of process parameters on dilution and aspect ratio	54
3.3.4	Multilayer deposition	56

3.3.4.1	Microstructural characterization	57
3.3.4.2	Microhardness tests.....	59
3.4	Conclusions.....	60
Chapter 4	Microstructure, mechanical, and tribological properties of DED-fabricated M2 HSS-B ₄ C composites	62
4.1	Introduction.....	63
4.2	Materials and methods	63
4.2.1	Materials	63
4.2.2	Sample preparation	65
4.2.3	Characterization	67
4.3	Results and discussion	70
4.3.1	Microstructure.....	70
4.3.2	Phase analysis	75
4.3.3	Density and relative density.....	76
4.3.4	Microhardness test	77
4.3.5	Reciprocating wear test.....	79
4.4	Conclusions.....	87
Chapter 5	Statistical modelling and optimization of machining process for DED-fabricated composite cutting tool inserts	90
5.1	Introduction.....	91
5.2	Materials and methods	92
5.2.1	Materials	92
5.2.2	Cutting tool insert preparation	92
5.2.3	Machining experiments.....	92

5.2.4	Response surface methodology.....	96
5.3	Results and discussion	97
5.3.1	Analysis of machining experimental data.....	98
5.3.2	Effect of process parameters on responses	103
5.3.2.1	Effect of cutting speed	107
5.3.2.2	Effect of feed rate.....	108
5.3.2.3	Effect of depth of cut	109
5.3.2.4	Effect of B ₄ C content	110
5.3.2.5	Effect of interactions.....	112
5.3.3	Multi-objective optimization	113
5.3.4	Machining performance at optimized conditions	115
5.4	Conclusions.....	121
Chapter 6	Effects of PVD coatings on machining performance of DED-fabricated composite cutting tool inserts	123
6.1	Introduction.....	124
6.2	Materials and methods	127
6.2.1	Coating deposition	127
6.2.2	Coating characterization	128
6.2.3	Machining experimentations.....	128
6.3	Results and discussion	128
6.3.1	Coating characterization	128
6.3.2	Machining experimentations.....	132
6.4	Conclusions.....	139
Chapter 7	Major conclusions and future scope	141

7.1	Conclusions.....	142
7.2	Future scope.....	145
	References.....	146
	List of Publications	180
	Biodata	182

List of Figures

Figure 1.1: Schematic of the hot-pressing process.	6
Figure 1.2: Schematic of the spark plasma sintering process.	8
Figure 1.3: Schematic of the microwave sintering process.	9
Figure 1.4: Schematic of the selective laser melting process.	12
Figure 1.5: Schematic of the directed energy deposition process.	14
Figure 1.6: Thesis-structure flowchart.	22
Figure 3.1: Fishbone diagram of laser-based DED processing parameters.	42
Figure 3.2: (a) Morphology and (b) Particle size distribution of M2 HSS powder.	44
Figure 3.3: (a) Schematic diagram and (b) experimental setup of the DED system.	46
Figure 3.4: Cross-sectional schematic of DED-deposited single bead.	46
Figure 3.5: DED-deposited M2 HSS single tracks.	49
Figure 3.6: Microscopic images of single-bead cross-sections showing the effect of laser power and scan speed at a constant powder feed rate.	49
Figure 3.7: Microscopic images of single-bead cross-sections showing the effect of powder feed rate at a constant laser power and scan speed.	50
Figure 3.8: Effect of scan speed on (a) bead width, (b) penetration depth, and (c) bead height at a given laser power, and (d) effect of powder feed rate at a constant power and scan speed.	53
Figure 3.9: Optical micrograph of single-bead depositions at laser powers of (a) 800 W and (b) 2400 W.	54
Figure 3.10: Effect of scan speed on (a) dilution and (b) aspect ratio at given laser power, and (c) effect of powder feed rate on dilution and aspect ratio at fixed laser power and scan speed.	55
Figure 3.11: Dilution vs aspect ratio map for different combinations of DED parameters.	56

Figure 3.12: Multilayer-deposited sample.	56
Figure 3.13: XRD pattern of M2 HSS sample.....	57
Figure 3.14: SEM micrograph in the BSE mode for (a) M2 HSS sample and its (b) magnified image of the deposition region.....	59
Figure 3.15: EDS mapping of M2 HSS sample.....	59
Figure 3.16: Microhardness plot of the M2 HSS sample.....	60
Figure 4.1: SEM morphology of powder materials: (a) M2 HSS, (b) B ₄ C, and (c) ball-milled M2 HSS-10 vol.% B ₄ C, and (d) EDS mapping of M2 HSS-10 vol.% B ₄ C powder.....	64
Figure 4.2: Schematic illustration of depositing samples using DED.	66
Figure 4.3: SEM micrograph of DED-fabricated M2 HSS-25 vol.% B ₄ C composite sample.....	67
Figure 4.4: (a) Schematic representation and (b) experimental setup of the reciprocating wear test.	69
Figure 4.5: SEM backscattered images showing microstructures of the deposited (a) S0, (b) S1, (c) S2, (d) S3, and (e) S4 samples.....	72
Figure 4.6: EDS analysis of (a) S0, (b) S1, (c) S2, (d) S3, and (e) S4 samples.....	74
Figure 4.7: XRD patterns of the fabricated samples.....	76
Figure 4.8: (a) Actual and relative densities of the deposited samples and (b) SEM micrograph of S0 and S4 samples.	77
Figure 4.9: Microhardness of the DED-fabricated samples.....	79
Figure 4.10: (a) Coefficient of friction (COF) with time, and (b) average COF of DED-fabricated samples.....	80
Figure 4.11: (a) Mass loss after wear test and (b) wear rate of the samples.	81
Figure 4.12: Wear track depth profiles of the samples after the wear test.	82
Figure 4.13: Wear track 3D profilometer for (a) S0, (b) S1, (c) S2, (d) S3, and (e) S4 samples.	83

Figure 4.14: SEM morphology of wear track at low and high magnifications for (a) S0, (b) S1, (c) S2, (d) S3, and (e) S4 after wear testing.....	86
Figure 4.15: SEM morphology of wear debris generated from samples (a) S0, (b) S1, (c) S2, (d) S3, and (e) S4 after wear test.....	87
Figure 4.16: Schematic of the wear mechanism.	87
Figure 5.1: Illustration of cutting inserts fabrication steps.	92
Figure 5.2: CNC lathe machine.	93
Figure 5.3: (a) Schematic of cutting insert, (b) DED-fabricated insert, and (c) tool holder.	93
Figure 5.4: Setup for measuring (a) cutting force, (b) surface roughness, and (c) tool wear.	95
Figure 5.5: (a) SEM microstructure and (b) XRD result of the workpiece material.	98
Figure 5.6: (a) Main effect plot and (b) percentage contribution for cutting force.	104
Figure 5.7: (a) 3D surface plot and (b) 2D interaction plot of feed rate and depth of cut for cutting force.	105
Figure 5.8: (a) Main effect plot and (b) percentage contribution for surface roughness.	105
Figure 5.9: (a) Main effect plot and (b) percentage contribution for tool wear.	106
Figure 5.10: (a) 3D surface plot and (b) 2D interaction plot of cutting speed and depth of cut for tool wear.	106
Figure 5.11: Tool flank wear at different cutting speeds.....	108
Figure 5.12: Tool flank wear at different feed rates.....	109
Figure 5.13: Tool flank wear at different depths of cut.....	110
Figure 5.14: Tool flank wear at different B ₄ C content in the tool material.	112
Figure 5.15: Pareto solutions obtained from the multi-objective optimization method.	115
Figure 5.16: Measured cutting force components relative to machining time.	117
Figure 5.17: Resultant cutting force for different cutting tools.	118
Figure 5.18: Surface roughness profiles after machining.	118

Figure 5.19: Average surface roughness values of the machined workpiece.....	119
Figure 5.20: Flank wear profiles after machining 20 mm length for all three cutting tools..	119
Figure 5.21: Maximum flank wear values for machining 20 mm length using all three tools.	120
Figure 6.1: Schematic illustration of the CAE-PVD process.	127
Figure 6.2: Cross-sectional micrographs of (a) TiN and (b) AlTiN coatings.	129
Figure 6.3: SEM surface morphologies of (a) TiN and (b) AlTiN coatings.	130
Figure 6.4: EDS analysis of (a) TiN and (b) AlTiN coatings.....	130
Figure 6.5: XRD patterns of the coated samples.	131
Figure 6.6: Microhardness of uncoated and coated tools.	132
Figure 6.7: Variation in cutting force components with machining time.	133
Figure 6.8: Resultant cutting force for uncoated and coated tools.	134
Figure 6.9: Surface roughness profiles of the machined surface.	135
Figure 6.10: Average surface roughness values comparison.	135
Figure 6.11: Flank wear images of cutting tools after machining 20 mm length.	136
Figure 6.12: Maximum flank wear values of cutting tools after machining 20 mm length. .	137
Figure 6.13: Tool life comparison of uncoated and coated tools.	138

List of Tables

Table 1.1: Comparison of major cutting tool fabrication processes [20–27].....	4
Table 1.2: Comparison of SLM versus DED.	15
Table 1.3: Comparison of CVD versus PVD.	18
Table 1.4: Comparison of different PVD techniques.	19
Table 3.1: Elemental compositions of the feedstock and substrate material (wt.%)	45
Table 3.2: Process parameters and measured responses of the single-bead depositions.	50
Table 4.1: Process parameters of DED utilized for all sample fabrication.	66
Table 4.2: Notations used for fabricated composite samples.	67
Table 4.3: Microhardness and wear rate comparison of M2 HSS-based composites.	83
Table 5.1: Chemical compositions of the workpiece material (wt.%)	94
Table 5.2: Levels and symbols of process parameters for the machining experiments.	97
Table 5.3: Details of experimental runs and the corresponding values of responses.	100
Table 5.4: ANOVA table for cutting force after removing insignificant terms.	101
Table 5.5: ANOVA table for surface roughness after removing insignificant terms.	102
Table 5.6: ANOVA table for tool wear after removing insignificant terms.	102
Table 5.7: Confirmatory experiments within the process parameter range.	103
Table 5.8: List of input parameters used for the optimization algorithm.	114
Table 5.9: Experiment performed at optimized process parameters.	115
Table 5.10: Comparison of the present study with existing literature.	120
Table 6.1: Comparison of common hard coating materials.	125
Table 6.2: Comparison of the present coating study with relevant literature.	138

Abbreviations

3D	Three dimensional
Al ₂ O ₃	Alumina
AlTiN	Aluminum titanium nitride
AM	Additive manufacturing
ANN	Artificial neural network
ANOVA	Analysis of variance
Ar	Argon
ASTM	American society for testing and materials
B ₂ O ₃	Boron oxide
B ₄ C	Boron carbide
BUE	Built-up edge
CAD	Computer-aided design
CAE	Cathodic arc evaporation
cBN	Cubic boron nitride
CCD	Central composite design
CEM	Composite extrusion modelling
CNC	Computer numerical control
CNT	Carbon nanotube
COF	Coefficient of friction
CVD	Chemical vapor deposition
DC	Direct current
DD	Diamond dust
DED	Directed energy deposition

DF	Degree of freedom
DFA	Desirability function approach
DIW	Direct ink writing
DMLS	Direct metal laser sintering
DOE	Design of experiment
ECD	Equivalent circle diameter
EDM	Electric discharge machining
EDS	Energy dispersive X-ray spectroscopy
FCC	Face-centered cubic
Fe ₃ C	Iron carbide or cemented carbide
FeB, Fe ₂ B	Iron boride
FESEM	Field-emission scanning electron microscope
FFF	Fused filament fabrication
GA	Genetic algorithm
GWO	Gray wolf optimizer
HIP	Hot isostatic pressing
HP	Hot pressing
HSS	High-speed steel
LPBF	Laser powder bed fusion
MEX	Material extrusion
MMC	Metal matrix composite
MOGA	Multi-objective genetic algorithm
MOPSA	Multi-objective Pareto search algorithm
MRR	Material removal rate
MS	Mean of squares

MWS	Microwave sintering
NSGA	Non-dominated sorting genetic algorithm
PECS	Pulsed electric current sintering
PM	Powder metallurgy
PVD	Physical vapor deposition
RSM	Response surface methodology
S/N ratio	Signal-to-noise ratio
SEM	Scanning electron microscope
SiC	Silicon carbide
SLM	Selective laser melting
SPS	Spark plasma sintering
SS	Sum of squares
STL	Stereolithography
TiN	Titanium nitride
WVGWO	Weighted value gray wolf optimizer
XRD	X-ray diffraction

Nomenclature

vol.%	Volume percentage
wt.%	Weight percentage
θ	Angle
W	Wear rate
V	Volume loss
F	Applied load
L	Total sliding distance
F_x	Radial force
F_y	Tangential force
F_z	Feed force
F_R	Resultant cutting force
R_a	Average surface roughness
VB	Tool flank wear
Y	Predicted output response variable
X_i, X_i^2, X_iX_j	First-order, second-order, and interaction terms of process parameters
$\beta_0, \beta_i, \beta_{ii}, \beta_{ij}$	Regression coefficients
k	Number of input variables
ε	Random error
Y'	Range of response variables
α	Significance level
V_ε	Variance of the total error
F_{value}	Fisher's value
R^2	Coefficient of determination

v	Cutting speed
f	Feed rate
d	Depth of cut